Generating Proxy SWOT Water Surface Elevations Using WRF-Hydro and the CNES SWOT Hydrology Simulator

Nicholas J. Elmer[1], Christopher Hain[2], Faisal Hossain[3], Damien Desroches[4], Claire Pottier[4]

[1] NASA Postdoctoral Program, NASA Marshall Space Flight Center, Huntsville, Alabama, USA

[2] Earth Science Office, NASA Marshall Space Flight Center, Huntsville, Alabama, USA

[3] Civil and Environmental Engineering, University of Washington, Seattle, Washington, USA

[4] Centre National d'Etudes Spatiales, Paris, France

Corresponding author: Nicholas J. Elmer, NASA Postdoctoral Program, NASA Marshall Space Flight Center, 320 Sparkman Drive, Huntsville, AL, 35805. Email: nicholas.j.elmer@nasa.gov

Key Points:

- Two approaches for generating proxy SWOT water surface elevations from a hydrology modeling framework are provided.
- Proxy SWOT data is well-suited for societal applications and scientific studies prior to and following launch.
- The Large-scale SWOT Hydrology Simulator provides realistic proxy SWOT data for error budget studies.

Abstract

The Surface Water Ocean Topography (SWOT) mission will launch in 2021 to provide the first global inventory of terrestrial surface water. Although SWOT is primarily a research mission with key science objectives in both the oceanography and hydrology domains, SWOT data is expected to have application potential to address many societal needs. To identify SWOT applications, prepare for the use of SWOT data, and quantify SWOT impacts prior to launch, realistic proxy SWOT observations with representative measurement errors are required. This paper provides a step-by-step description of two methods for deriving proxy SWOT water surface elevations (WSE) from an Observing System Simulation Experiment (OSSE) using the Weather Research and Forecasting hydrological extension package (WRF-Hydro). The first, a basic method, provides a simple and efficient way to sample WRF-Hydro output according to the SWOT orbit and add random white noise to simulate measurement error, similar to many previous approaches. An alternate method using the Centre National d'Etudes Spatiales (CNES) Large-scale SWOT Hydrology Simulator accounts for additional sources of measurement error and produces output in formats comparable to that expected from official SWOT products. The basic method is ideal for river hydrology applications in which a full representation of SWOT measurement errors and spatial resolution are unnecessary, whereas the CNES simulator approach is better-suited for more rigorous scientific studies that require a comprehensive error budget.

Plain Language Summary

The Surface Water Ocean Topography (SWOT) mission is a multi-national satellite mission that is expected to launch in 2021 to observe global rivers, lakes, reservoirs, and wetlands. As the

first of its kind to measure inland water, SWOT is expected to address many societal needs. To identify SWOT applications, prepare for the use of SWOT data, and quantify SWOT impacts prior to launch, realistic sample SWOT observations are needed. This paper provides a step-by-step description for deriving proxy SWOT measurements using a hydrologic model and a SWOT observation simulator.

1. Introduction

The Surface Water Ocean Topography (SWOT) mission (Biancamaria et al. 2016) will provide the first global inventory of terrestrial surface water in rivers, lakes, and wetlands following launch in 2021. SWOT is a joint mission between the National Aeronautics and Space Administration (NASA), Centre National d'Etudes Spatiales (CNES), Canadian Space Agency, and the United Kingdom Space Agency supporting several instruments, including a nadir altimeter and a bistatic Ka-band (35.75 GHz) Radar Interferometer (KaRIn) (Fjørtoft et al. 2014). The nadir altimeter continues the legacy of nadir altimetry satellite missions that began with Topography Experiment/Poseidon (1992-2006) and followed by the Jason series (2001-present) and IceSAT missions (2003-present; Zhang et al. 2011; O'Loughlin et al. 2016). These missions have provided global, point-based observations of ocean surface topography using nadir-profiling dual-frequency altimeters at C-band (5.3 GHz) and Ku-band (13.6 GHz), resulting in observations at low spatial resolutions of 200-400 m along track and height resolution of 10-50 cm over ocean. Although a few studies have shown that these nadir radar altimetry missions can monitor terrestrial water bodies such as inland rivers, lakes, and wetlands (e.g., Kouraev et al. 2004, Papa et al. 2010, Biancamaria et al. 2017), the lower frequencies degrade the spatial and

altimetric resolution and is a major limitation for monitoring small or narrow terrestrial water bodies (Alsdorf et al. 2007, Biancamaria et al. 2016, Altenau et al. 2016).

KaRIn is a wide-swath instrument (0.6-4.1° incidence angles) providing near-global, high-resolution measurements of water surface elevation (WSE, the height of the river surface above a reference geoid), width, and slope across the 120 km swath for rivers with widths greater than 100 m, but possibly down to 50 m (Biancamaria et al. 2016, Pavelsky et al. 2014, Rodriguez 2016). KaRIn builds on the heritage of the nadir altimeters listed previously and the Shuttle Radar Topography Mission (SRTM; Enjolras and Rodriguez 2009), which supported swath topography measurements at C-band and X-band. However, SRTM lacked global coverage and had very low vertical accuracy (Alsdorf et al. 2007). Other Ka-band satellite instrument to have flown include the GPM Dual-frequency phased-array Precipitation Radar (Hou et al. 2014) and the Satellite for ARgos and ALtika (SARAL) (Biancamaria et al. 2017) which were primarily designed to observe precipitation and ocean topography, respectively, rather than terrestrial surface water. In using Ka-band instead of lower frequency bands (e.g., C-band or Ku-band), SWOT can gather measurements at a finer spatial resolution with less penetration into soil, snow, and vegetation (Fjørtoft et al. 2014, Biancamaria et al. 2016). Therefore, KaRIn is unique in that it will be the first satellite instrument to fully resolve terrestrial surface water bodies with high altimetric accuracy.

SWOT data products will be made available on the Physical Oceanography Distributed Active Archive Center (PO.DAAC) and a CNES distribution center after launch (PO.DAAC 2020). SWOT Level 2 data products include the water mask (as a geolocated point cloud), estimated WSE, WSE uncertainty, and estimated surface area (Rodriguez 2016). From this are

derived a global set of vectors denoting rivers with location, inundated area and extent, WSE, slope, width, and discharge, including uncertainties for all quantities (Rodriguez 2016).

Error in the SWOT measurements will come from several sources: instrument thermal (white) noise, error in the interferometric baseline length and roll angle, wet and dry tropospheric effects, ionospheric effects, crustal vertical motions due to solid Earth and pole tides, and topographic and vegetation layover (Fu and Rodriguez 2004; Durand et al. 2008; Enjolras and Rodriguez 2009, Biancamaria et al. 2017). Additional and potentially large errors arise during processing, with pixel misclassification while calculating the water mask (Biancamaria et al. 2016) or phase unwrapping due to height ambiguity (Rosen et al. 2000; Fjørtoft et al. 2014). Thermal noise is the only significant source of error that can be reduced through pixel averaging. In current baseline SWOT processing, height errors due to thermal noise are expected to be between 0.5 – 3 m at the pixel level (Durand et al. 2008, 2010; Yoon et al. 2012; Biancamaria et al. 2016), but can be reduced to 4 cm with pixel averaging for a 1 km^2 water body and nearly 0 cm for a very large water body (Enjolras et al. 2006; Durand et al. 2014; Andreadis and Schumann 2014; Munier et al. 2015). The native spatial resolution for KaRIn is approximately 6 m in the along-track direction and 60 m (near range) to 10 m (far range) in the across-track direction (Biancamaria et al. 2016).

SWOT is primarily a research mission, but the data will also prove useful for societal applications. With a mission lifetime of only three years, it is imperative that potential SWOT applications are identified and the impacts of using SWOT measurements for these applications are quantified prior to launch in order to obtain as much benefit from this unique mission as possible. In lieu of real SWOT measurements, proxy SWOT datasets which mimic SWOT sampling and measurement error are needed for both science and applications.

One source of proxy data is from AirSWOT (Altenau et al. 2016; Pitcher et al. 2019), an airborne SWOT analogue developed to provide proxy SWOT data and act as the primary calibration, validation, and science support instrument for the SWOT mission. AirSWOT contains a multi-baseline Ka-band interferometric synthetic aperture radar known as the Ka-band SWOT Phenomenology Airborne Radar (KaSPAR), which collects topographic maps of water surfaces and floodplains in the same manner as the SWOT KaRIn (Altenau et al. 2016, Pitcher et al. 2019). The main differences between SWOT KaRIn and AirSWOT KaSPAR are that KaSPAR has outer swath incidence angles ranging from 4°–25° and is an airborne instrument, flying on a B200 Super King Air aircraft at an altitude of 8 km (Altenau et al. 2016). These differences in incidence angles and viewing geometry make AirSWOT observations substantially different than those expected from SWOT, but still provide accurate SWOT-quality measurements of WSE (Altenau et al. 2016).

While AirSWOT measurements are useful in preparing for the SWOT mission, the measurements are geographically limited and only available for select time periods. Therefore, for most pre-launch studies, proxy data must be generated using an Observation System Simulation Experiment (OSSE). To date, proxy SWOT datasets have been used to quantify assimilation impacts on river modeling (Andreadis et al. 2007; Biancamaria et al. 2011) and reservoir management (Munier et al. 2015), develop procedures for estimating river bathymetry and discharge (Durand et al. 2008, 2010, 2014; Yoon et al. 2012; Bonnema et al. 2016), optimize hydrologic model parameters (Pedinotti et al. 2014), and represent SWOT spatial and temporal coverage for complementing existing in situ gauge networks (Pavelsky et al. 2014).

This paper demonstrates two methods for deriving proxy SWOT WSE from an OSSE using the Weather Research and Forecasting hydrological extension package (WRF-Hydro;

Gochis et al. 2018) and the CNES Large-Scale SWOT Hydrology Simulator (CNES 2020). Step-by-step descriptions for both processes are given to encourage broader use by the science and applications community. While SWOT is designed for both ocean and terrestrial surface water studies, this paper only considers the terrestrial surface water constituent. Unlike ocean applications where the SWOT error budget is simpler and well-understood, further understanding of the error budget for terrestrial water detection and measurement is needed to fully appreciate SWOT capabilities. Thus, this paper provides a timely and critical service in enabling the SWOT user and research communities to build up expertise in the use of SWOT data, engage key science questions, and address potential societal applications prior to launch.

2. Data and Methods

2.1. WRF-Hydro OSSE Configuration

This study uses a WRF-Hydro OSSE to generate proxy SWOT WSE. WRF-Hydro is a high-resolution hydrologic routing and streamflow modeling framework which couples column land surface, terrain routing, and channel routing models (Figure 1). Furthermore, WRF-Hydro is a fully-distributed, multi-physics, multi-scale hydrologic and hydraulic modeling system, enabling it to represent processes on spatial scales ranging from catchment to continent (Gochis et al. 2018, Yucel et al. 2015, Senatore et al. 2015). WRF-Hydro is based upon research applications over watershed and basin scales both in the United States and around the world (Fersch et al. 2014, Yucel et al. 2015, Senatore et al. 2015, Fredj et al. 2015, Givati et al. 2016, Arnault et al. 2016, Naabil et al. 2017, Kerandi et al. 2018, Lin et al. 2018), making it a well-documented and attractive hydrologic modeling framework for both hydrology research and operational hydrologic forecasting. For example, the National Oceanic and Atmospheric

157 Administration (NOAA) Office of Water Prediction (OWP) implemented an operational, high-
158 resolution National Water Model (NWM; NOAA Office of Water Prediction 2019) as an
159 instantiation of WRF-Hydro.

160 The Noah land surface model with Multi-Parameterization options (Noah-MP; Niu et al.
161 2011) is configured as the WRF-Hydro land surface model with a 1 km spatial resolution. The
162 WRF-Hydro terrain routing grid is created at a spatial resolution of 100 m. The WRF-Hydro
163 terrain and channel routing grids are derived from the WRF-Hydro GIS Pre-processing Toolkit
164 v5.1 (Sampson and Gochis 2015) using the Weather Research and Forecasting (WRF;
165 Skamarock et al. 2008) Pre-processing System (WPS) GEOGRID file and the National Elevation
166 Dataset (NED; U. S. Geological Survey 2017) Digital Elevation Model (DEM). Meteorological
167 forcing for WRF-Hydro is obtained by regridding the Global Land Data Assimilation System
168 Version 2 (GLDAS-2; Rodell et al. 2004) forcing to a 1 km resolution to match the Noah-MP
169 resolution. Selected model parameterization options are listed in Table 1. Note that the diffusive
170 wave gridded channel routing option must be used when generating proxy SWOT WSE in order
171 to obtain the required variables without performing custom modifications to the source code.

172 The upper Tanana River (upstream of Nenana, Alaska and includes Fairbanks, Alaska)
173 and the Susitna River basin in Southcentral Alaska are considered, which contain few in situ
174 observations but a large number of SWOT observable rivers (Figure 2). Proxy SWOT
175 observations of WSE are generated for the Tanana River during June 2015 (a low-flow case)
176 following a five-year spin-up period and for the Susitna River during September 2012 (a high-
177 flow case) following a four-year spin-up period. This study uses WRF-Hydro version 5.0.3
178 (Gochis et al. 2018) with parameter values borrowed from a calibration of the Chena River basin,
179 which falls within the Tanana River basin. For this analysis, the WRF-Hydro model output

represents reality, therefore considered truth and free of error, while derived proxy SWOT measurements contain measurement errors. Thus, while calibration may not be transferrable between basins and a thorough calibration is typically necessary to achieve the best model performance, a representative (estimated) calibration is sufficient for this study in order to demonstrate methods of deriving proxy SWOT WSE.

2.2. Generating Proxy SWOT WSE

WRF-Hydro provides the geolocation (latitude and longitude) of each channel point along with channel elevation ($z_{channel}$) and channel head (h). A basic method for creating proxy SWOT WSE is to add random white noise representative of SWOT measurement error and then sample the corrupted measurements according to the SWOT orbit parameters. A similar process is followed by many heritage SWOT studies (e.g., Andreadis et al. 2007, Durand et al. 2008, 2010, Biancamaria et al. 2011, Munier et al. 2015).

Step 1: From WRF-Hydro output, calculate WSE_{True}:

$$WSE_{True} = z_{channel} + h. \qquad (1)$$

Recall that WSE_{True} is assumed error free.

Step 2: Generate random white noise (h') is using the equation:

$$h' = N\left(0, \frac{\sigma_z}{\sqrt{n_{pixels}}}\right), \qquad (2)$$

in which h' is sampled by a zero mean Gaussian model (N) with random errors with a height standard deviation (σ_z) of 50 cm (Durand et al. 2008, 2010; Yoon et al. 2012; Biancamaria et al. 2016) and where n_{pixels} is the number of SWOT pixels that would be contained within each model gridpoint (Durand et al. 2010). Since SWOT spatial resolution after pixel averaging (to reduce altimetric error) will be approximately 21 m in the along-track direction and 60-10 m in

the cross-track direction as incidence angle increases. For simplicity, a 50 m resolution in both the along-track and cross-track directions is used in this paper, resulting in n_{pixels}=4 for the 100 m resolution model grid. Thus, the random error at a resolution of 100 m (h'_{100m}) becomes:

$$h'_{100m} = N(0, 25\ cm). \qquad (3)$$

Step 3: Calculate the proxy SWOT WSE ($WSE'_{WRFHydro}$) from h using the equation:

$$WSE'_{WRFHydro} = WSE_{True} + h'_{100m}. \qquad (4)$$

Step 4: To obtain $WSE'_{WRFHydro}$ with appropriate SWOT orbit characteristics, sample $WSE'_{WRFHydro}$ according to the CNES proxy SWOT orbit (Aviso+ 2015), which is based on an orbit inclination of 78°. For each projected SWOT overpass, sample $WSE'_{WRFHydro}$ points falling within cross-track distances of 10-60 km, matching the SWOT measurement range.

Step 5: Further sampling based on river width is required, since SWOT can only observe rivers with widths greater than 50 m. For this work, Strahler streamorder (Strahler 1957) is used as a proxy. A relative comparison between streamorder derived from the WRF-Hydro GIS Pre-processing Toolkit and the Global River Width from Landsat (GRWL; Allen and Pavelsky 2018) dataset suggests that a streamorder greater than or equal to five serves as a decent method for selecting rivers with widths greater than 50 m (Figure 2). Thus, only channel points for rivers with a streamorder greater than or equal to five are extracted for this analysis. Reach-level $WSE'_{WRFHydro}$ are obtained by sampling the midpoint WSE for each reach of the WRF-Hydro channel network. Channel reaches are defined by the WRF-Hydro GIS Pre-processing Toolkit.

2.3. CNES SWOT Hydrology Simulator

Alternatively, proxy SWOT WSE can be generated from WSE_{True} (Equation 1) using the CNES SWOT Large-Scale Hydrology Simulator, which is made publicly available by CNES

(2020). The CNES simulator not only accounts for random white noise (like the basic method in Section 2.2), but also dark water effects, uncertainty due to satellite position, geolocation errors, and tropospheric effects. The simulator ignores vegetation and topographic layover effects, which are potentially large for near-nadir instruments like SWOT. However, layover effects are expected to be mitigated with SWOT by relying on the strong contrast between land and water surfaces at Ka-band (citations). A spherical earth is assumed which reduces accuracy above 60° latitude and phase unwrapping is idealized. Although the CNES simulator is a large-scale simulator without full error representation, it is sophisticated enough to enable hydrology error budget studies and provide realistic proxy SWOT data. Elmer (2020) provides a detailed user tutorial for configuring and running the CNES simulator, but the main steps are briefly described here.

Step 1: The CNES SWOT Hydrology Simulator calculates proxy SWOT WSE based on a river polygon shapefile containing WSE information (CNES 2020, Elmer 2020). The WRF-Hydro GIS Pre-processing Toolkit optionally creates a river polyline shapefile for a WRF-Hydro domain, which can be converted to a river polygon shapefile using the ArcGIS (ESRI 2018) Buffer tool. However, a river polygon shapefile can be created without the WRF-Hydro GIS Pre-processing Toolkit simply using ArcGIS Spatial Analyst Hydrology toolbox, which is described by Elmer (2020). Similar tools are available in QGIS (QGIS Development Team 2020), although the WRF-Hydro GIS Pre-processing Toolkit is only compatible with ArcGIS (Sampson and Gochis 2015).

Step 2: For compatibility with the CNES simulator, the polygon shapefile must contain water surface height (HEIGHT) and river flag (RIV_FLAG) attributes. RIV_FLAG must be set

to 1 for river segments, but 0 for polygons representing lakes or reservoirs along the river network. HEIGHT is assigned from the model using WSE_{True}.

Step 3: Running the CNES simulator creates a pixel cloud of proxy SWOT WSE (WSE'_{PixC}) accounting for the represented error sources and sampled according to the CNES proxy SWOT orbit (Aviso+ 2015). In particular, WSE'_{PixC} simulates the variability of pixel size and pixel error across the SWOT swath, which can impact the observability of a given reach or lake. Random height error (σ_{h_raw}) is described in a hard-coded file within the simulator, for a 10 dB hypothesis of water back-scattering and a presuming factor of 2.125. This error depends on the incidence angle and is the pixel-wise error without averaging. A noise multiplier factor (k) is then applied to simulate the four-look-azimuth averaging performed during processing, by default set to $4^{-1/2} = 0.5$. Thus, the azimuth-averaged random height error (σ_{h_ave}) is given as:

$$\sigma_{h\_ave} = k\sigma_{h\_raw} \qquad (5)$$

Then during simulation, for each pixel accounting for its incidence angle, a random Gaussian error is simulated with a σ_{h_ave} variance.

WSE'_{PixC} were post-processed to derive a reach-averaged product ($WSE'_{ReachAvg}$) based on reaches defined by the WRF-Hydro GIS Pre-processing Toolkit. Sampling at each reach is useful for applications that cannot process the full resolution pixel cloud (e.g., data assimilation and calibration). This reach-averaged product also mimics the sampling of the reach-averaged discharge product that will be available from PO.DAAC and CNES following launch. However, unlike reach-averaged discharge, reach-averaged WSE more accurately describes the midpoint of the reach rather than the whole reach, since WSE can vary greatly even within a single reach. Thus, $WSE'_{ReachAvg}$ is only shown in this paper to demonstrate the spatial coverage of the reach-averaged SWOT products which will be available in the future from PO.DAAC.

3. Results

Figure 3 shows reach-level $WSE'_{WRFHydro}$ for a full SWOT swath over the Susitna basin with proxy WSE derived following the basic method. Since only random white noise is added to WSE_{True} in this case, all other expected SWOT measurement error sources are neglected, which is a significant disadvantage of this approach. However, the simplicity of the basic method requires no pre-processing, but can directly operate on WRF-Hydro (or any other hydrology modeling framework that captures surface water dynamics) output files. The method is also computationally inexpensive due to the error simplifications. Ideal applications of this method are those that do not require full representation of SWOT measurement error or full SWOT spatial resolution, such as examining SWOT spatial and temporal coverage for a WRF-Hydro domain or developing data assimilation or calibration frameworks to ingest future SWOT products (e.g., Elmer 2019).

The CNES simulator captures several additional sources of measurement error beyond random white noise and thus has the advantage of providing more representative proxy SWOT WSE. Figure 4 compares WSE'_{PixC} and $WSE'_{ReachAvg}$. The sampling of $WSE'_{ReachAvg}$ is very similar to the reach-level $WSE'_{WRFHydro}$ shown in Figure 3. However, WSE'_{PixC} represents the full resolution of the SWOT pixel cloud, providing multiple measurements for each river cross-section. Thus, the use of the CNES simulator to derive proxy SWOT WSE from any model output or in situ observations is better suited for scientific studies in which high-resolution measurements are needed, such as those investigating river properties and surface water dynamics (e.g., Garambois et al. 2015, Pitcher et al. 2019).

Figure 5 compares $WSE'_{ReachAvg}$ with WSE_{True} for several points within the Susitna and Tanana basins (locations indicated in Figure 2). Although SWOT will observe higher latitudes more frequently than lower latitudes due to its 78° inclination, at similar latitudes the positioning of the SWOT swath and nadir gaps determines the number of observations. Thus, reach H located near the mouth of the Susitna River falls in several nadir gaps and is therefore observed only once during September 2012, whereas reach E is observed six times. Another significant characteristic of SWOT observations is the irregular temporal frequency, which is also noted by Biancamaria et al. (2016). For example, reach E is observed six times during the 30-day period, but some observations are separated in time by less than one day whereas others are as many as nine days apart. Thus, a flow event with a duration of eight days may be sampled twice or not at all depending on its timing with respect to the SWOT observations.

In terms of accuracy, $WSE'_{ReachAvg}$ visually compares well with WSE_{True}, capturing may of the changes in river elevation observed in the hydrographs. Yet several $WSE'_{ReachAvg}$ values have large deviations from WSE_{True}, most notably in Figure 5D, which is more than one meter above the WSE_{True}. However, only basic processing was performed to calculate $WSE'_{ReachAvg}$ for this case. Reach-averaged SWOT products which will be available from PO.DAAC will undergo more extensive processing and will provide quality flags and estimated uncertainty for each observation. Thus, errant points such as seen in Figure 5 can be screened prior to use in any research or societal application. A notable feature in the hydrographs for the Tanana River in Figure 5 (hydrographs A-D) are the diurnal oscillations mainly observed in the latter half of June 2015. Since this is a low-flow event, changes in streamflow are driven almost entirely by snowmelt, which naturally follows diurnal heating. Thus, these oscillations are expected and demonstrate that WRF-Hydro is capturing snowmelt-induced streamflow.

4. Conclusions

Two methods are presented for generating proxy SWOT WSE: a basic method and an approach using the CNES SWOT Hydrology Simulator. While the basic method is simple and computationally inexpensive, it requires the use of a hydrology modeling framework that can generate water surface dynamics and only accounts for random white noise. On the other hand, the CNES SWOT Hydrology Simulator is more flexible and represents many sources of measurement error (random white noise, tropospheric effects, roll angle error, dark water effects, and geolocation errors), but it requires an increased effort in properly preparing input datasets. The basic method is well-suited for applications where a full representation of SWOT measurement error or spatial resolution is not needed, such as examining SWOT spatial and temporal coverage of an area of interest for most data assimilation and calibration studies, whereas the CNES simulator approach is needed for more intensive scientific studies. The CNES simulator provides representative SWOT products with a good estimate of the error budget and can be quickly run over large areas, but neglects topographic effects. Thus, for rigorous error budget studies, the Jet Propulsion Laboratory RiverObs (Jet Propulsion Laboratory 2020) SWOT Simulator should be used in conjunction with the CNES simulator. The RiverObs simulator usually cannot be run over large areas since it is computationally expensive, but it can operate on CNES simulator output more efficiently and quickly.

For any river hydrology application, channel head or discharge is likely more useful than WSE. However, the uncertainty of derived channel head or discharge is a product of the uncertainty in channel bed elevation and bathymetry. For the examples shown in this paper, the channel elevation and bathymetry are perfectly known because these are explicit WRF-Hydro

parameters. However, deriving channel head or discharge from real SWOT WSE measurements will contribute additional uncertainty. Many studies (Durand et al. 2008, 2010, 2014; Yoon et al. 2012; Allen and Pavelsky 2018) have developed methods to estimate channel elevation and bathymetry to reduce potential uncertainty in derived SWOT products.

Future work will seek to replace the use of Strahler streamorder as a proxy for river width with the GRWL (Allen and Pavelsky 2018) river width dataset, which is expected to be the basis of SWOT river vector products. Furthermore, since WRF-Hydro is the basis of the current contiguous United States (CONUS) and future Alaska configurations of the NWM, future efforts building on Elmer (2019) can seek to quantify SWOT data assimilation and calibration impacts on NWM performance using proxy SWOT observations derived using the methods shown here.

For SWOT, and any unique satellite mission with a short lifetime, proxy data is essential in preparing to use new observations and maximizing mission impacts and societal benefits. Even after real SWOT data becomes available following launch, the need for proxy data will remain. There will still be value in generating proxy SWOT data for a broad range of activities, including simulated hydrology work and studies, software development, testing exercises, and education and outreach activities. Additionally, any future missions supporting instruments similar to KaRIn would benefit from proxy observations generated in a similar manner as the methods demonstrated here. Thus, the relevance of this work is not limited to the interim, but rather extends through and beyond the SWOT mission lifetime.

Acknowledgements. This work was funded by NASA Headquarters under the NASA Postdoctoral Program at NASA Marshall Space Flight Center administered by Universities Space Research Association. All software and model input data can be obtained freely online and

are cited in the references. Data used in the creation of figures is available at https://github.com/njelmer/proxySWOT.

References

Allen, G. H., and T. M. Pavelsky (2018), Global extent of rivers and streams, Science, 361, 6402, 585-588, doi:10.1126/science.aat0636.

Alsdorf, D. E., E. Rodriguez, and D. P. Lettenmaier (2007), Measuring surface water from space, Rev. Geophys., 45, RG2002, doi:10.1029/2006RG000197.

Altenau, E. H., T. M. Pavelsky, D. Moller, C. Lion, L. H. Pitcher, G. H. Allen, P. D. Bates, S. Calmant, M. Durand, and L. C. Smith (2016), AirSWOT measurements of river water surface elevation and slope: Tanana River, AK, Geophys. Res. Lett., 43, doi:10.1002/2016GL071577.

Andreadis, K. M., E. A. Clark, D. P. Lettenmaier, and D. E. Alsdorf (2007), Prospects for river discharge and depth estimation through assimilation of swath-altimetry into a raster-based hydrodynamics model, Geophys. Res. Lett., 34(L10403), 1-5, doi:10.1029/2007GL029721.

Andreadis, K. M. and G. J. P. Schumann (2014), Estimating the impact of satellite observations on the predictability of large-scale hydraulic models. Adv. Water Resour., 73, 44-54, doi:10.1016/j.advwatres.2014.06.006.

Arnault, J., S. Wagner, T. Rummler, B. Fersch, J. Bliefernicht, S. Andresen, and H. Kunstmann (2016), Role of Runoff–Infiltration Partitioning and Resolved Overland Flow on Land–Atmosphere Feedbacks: A Case Study with the WRF-Hydro Coupled Modeling System for West Africa. *J. Hydrometeor*., 17, 1489–1516, doi:10.1175/JHM-D-15-0089.1.

Aviso+ (2015), SWOT orbit, https://www.aviso.altimetry.fr/en/missions/future-missions/swot/orbit.html, accessed 8 September 2015.

Biancamaria., S., M. Durand, K. M. Andreadis, P. D. Bates., A. Boone, N. M. Mognard, and E. A. Clark (2011), Assimilation of virtual wide swath altimetry to improve Arctic river modeling, Remote Sens. Environ., 115(2), 373-381, doi:10.1016/j.rse.2010.09.008.

Biancamaria, S., F. Frappart, A.-S. Leleu, V. Marieu, D. Blumstein, J. D., Desjonqueres, F. Boy, A. Sottolichio, and A. Valle-Levinson (2016), Satellite radar altimetry water elevations performance over a 200 m wide river: Evaluation over the Garonne River, Advances in Space Research, 59(2017), 128-146, doi:10.1016/j.asr.2016.10.008.

Biancamaria, S., F. Frappart, A.-S. Leleu, V. Marieu, D. Blumstein, J. D., Desjonqueres, F. Boy, A. Sottolichio, and A. Valle-Levinson (2017), Satellite radar altimetry water elevations performance over a 200 m wide river: Evaluation over the Garonne River, Advances in Space Research, 59(2017), 128-146, doi:10.1016/j.asr.2016.10.008.

Cunge, J. A. (1969), On the subject of a flood propagation computation method (Muskingum method), J. Hydraul. Res., 7, 205-230.

CNES (2020), SWOT Hydrology Toolbox, https://github.com/CNES/swot-hydrology-toolbox.

Durand, M. K., K. M. Andreadis, D. E. Alsdorf, D. P. Lettenmaier, D. Moller, and M. Wilson, 2008: Estimation of bathymetric depth and slope from data assimilation of swath altimetry into a hydrodynamic model. Geophys. Res. Lett., 35 (L20401), 1-5, doi:10.1029/2008GL034150.

Durand, M., E. Rodriguez, D. E. Alsdorf, and M. Trigg (2010), Estimating river depth from remote sensing swath interferometry measurements of river height, slope and width,

IEEE. J. Sel. Top. Appl. Earth Observ. Remote Sens., 3(1), 20-31, doi:10.1109/JSTARS.2009.2033453.

Durand, M., J. Neal, E. Rodriguez, K. M. Andreadis, L. C. Smith, and Y. Yoon (2014), Estimating reach-averaged discharge for the River Severn from measurements of river water surface elevation and slope, J. Hydrol., 5111, 92-104, doi:10.1016/j.jhydrol.2013.12.050.

Elmer, N. J. (2019), Using satellite observations of river height and vegetation to improve National Water Model initialization and streamflow prediction, Ph.D. dissertation, Department of Atmospheric Science, The University of Alabama in Huntsville, Huntsville, Alabama, 113 pp, search.proquest.com/openview/d5a7c6483abcbedb8e18e8e043fe6a7c/.

Elmer, N. J. (2020), CNES Large Scale SWOT Simulator User's Tutorial for Terrestrial Surface Water Applications, 18 pp., https://github.com/njelmer/swot-hydrology-toolbox/blob/master/CNES-SWOT-Terrestrial-Hydrology-Simulator_Users-Tutorial.pdf.

Enjolras, V. M. and E. Rodriguez (2009), An assessment of a Ka-band radar interferometer mission accuracy over Eurasian Rivers. IEEE Transactions on Geoscience and Remote Sensing, 47 (6), 1752-1765, doi:10.1109/TGRS.2008.2006370.

ESRI 2018, ArcGIS Desktop: Release 10.6. Redlands, CA, Environmental Systems Research Institute.

Fersch, B., D. J. Gochis, H. Kunstmann, G. Mendicino, and A. S. (Eds.) (2014), Book of abstracts of the 1st European fully coupled atmospheric-hydrologic modeling and WRF-Hydro Users Workshop, Univ. of Calabria, Rende (CS), Italy.

Fjørtoft R, Gaudin JM, Pourthie N, Lalaurie JC, Mallet A, Nouvel JF, Martinot-Lagarde J, Oriot H, Borderies P, Ruiz C, Daniel S (2014), KaRIn on SWOT: characteristics of near-nadir Ka-band interferometric SAR imagery. IEEE Trans Geosci Remote Sens 52(4):2172–2185, doi:10.1109/TGRS.2013.2258402.

Fredj, E., M. Silver, and A. Givati (2015), An integrated simulation and distribution system for early flood warning, Int. J. Comp. Info. Tech., 4 (05), 517-526.

Fu, L. L., and E. Rodriguez (2004), High-resolution measurement of ocean surface topography by radar interferometry for oceanographic and geophysical applications, The state of the planet: frontiers and challenges in geophysics, R. S. J. Sparks and C. J. Hawkesworth, Eds., Geophysical Monograph 150, American Geophysical Union, Washington, 209-224, doi:10.1029/150GM17.

Garambois, P.-A., and J. Monnier (2015), Advances in water resources inference of effective river properties from remotely sensed observations of water surface, Advances in Water Resources, 79, 103-120, doi:10.1016/j.rse.2005.10.027.

Givati, A., D. Gochis, T. Rummler, and H. Kunstmann (2016), Comparing one-way and two-way coupled hydrometeorological forecasting systems for flood forecasting in the Mediterranean region, Hydro., 3 (6), 19, doi:10.3390/hydrology3020019.

Gochis, D.J., M. Barlage, A. Dugger, K. FitzGerald, L. Karsten, M. McAllister, J. McCreight, J. Mills, A. RafieeiNasab, L. Read, K. Sampson, D. Yates, W. Yu, (2018). The WRF-Hydro modeling system technical description, (Version 5.0). NCAR Technical Note. 107 pages. Available online at https://ral.ucar.edu/sites/default/files/public/WRF-HydroV5TechnicalDescription.pdf. Source Code DOI:10.5065/D6J38RBJ.

446 Hou, A. Y., and Coauthors (2014), The Global Precipitation Measurement mission. Bull. Amer.
447 Meteor. Soc., 95, 701–722, doi:10.1175/BAMS-D-13-00164.1.
448 Jet Propulsion Laboratory (2020), RiverObs, https://github.com/SWOTAlgorithms/RiverObs,
449 accessed 13 January 2020.
450 Kerandi, N., J. Arnault, P. Laux, et al. (2018), Joint atmospheric-terrestrial water balances for
451 East Africa: a WRF-Hydro case study for the upper Tana River basin, *Theor. Appl.*
452 *Climatol.* 131, 3-4, 1337-1355, doi:10.1007/s00704-017-2050-8.
453 Kouraev, A. V., E. A. Zakharova, O. Samain, N. M. Mognard, and A. Cazenave (2004), Ob river
454 discharge from TOPEX/Poseidon satellite altimetry (1992–2002), Remote Sens.
455 Environ., 93, 238-245.
456 Lin, P., Z.-L. Yang, D. J. Gochis, W. Yu, D. R. Maidment, M. A. Somos-Valenzuela, C. H.
457 David (2018), Implementation of a vector-based river network routing scheme in the
458 community WRF-Hydro modeling framework for flood discharge simulation,
459 *Environmental Modelling & Software*, 107, 1-11, doi:10.1016/j.envsoft.2018.05.01.
460 McCuen, R. H., Z. Knight, and A. G. Cutter (2006), Evaluation of the Nash–Sutcliffe efficiency
461 index, J. Hydrol. Eng., 11(6), 597–602, doi:10.1061/(ASCE)1084-0699(2006)11:6(597).
462 Munier, S., A. Polebistki, C. Brown, G. Belaud, and D. P. Lettenmaier (2015), SWOT data
463 assimilation for operational reservoir management on the upper Niger River Basin, Water
464 Resour. Res., 51, 554-575, doi:10.1002/2014WR016157.
465 Naabil, E., B. L. Lamptey, J. Arnault, A. Olufayo, and H. Kunstmann (2017), Water resources
466 management using the WRF-Hydro modelling system: Case-study of the Tono dam in
467 West Africa, J. Hydrology, 12, 196-209, doi:10.1016/j.ejrh.2017.05.010.

NCAR (2020), WRF-Hydro modeling system, National Center for Atmospheric Research Research Applications Laboratory, https://www.ral.ucar.edu/projects/wrf_hydro.

Niu, G.-Y., Z.-L. Yang, K. E. Mitchell, F. Chen, M. B. Ek, M. Barlage, A. Kumar, K. Manning, D. Niyogi, E. Rosero, M. Tewari, and Y. Xia (2011), The community Noah land surface model with multiparameterization options (Noah-MP): 1. Model description and evaluation with local-scale measurements, J. Geophys. Res., 116(D12109), doi:10.1029/2010JD015139.

NOAA Office of Water Prediction (2019), The National Water Model, http://water.noaa.gov/about/nwm, accessed 16 May 2019.

O'Loughlin, F. E., J. Neal, D. Yamazaki, and P. D. Bates (2016), ICESat-derived inland water surface spot heights, Water Resour. Res., 52, 3276-3284, doi:10.1002/2015WR018237.

PO.DAAC (2020), Available online [https://podaac.jpl.nasa.gov/] from NASA EOSDIS PO.DAAC, Pasadena, CA, Accessed January 15, 2020.

Papa, F., F. Durand, W. B. Rossow, A. Rahman, and S. K. Bala (2010), Satellite altimeter-derived monthly discharge of the Ganga-Brahmaputra River and its seasonal to interannual variations from 1993 to 2008, J. Geophys. Res., 115(C12013), doi:10.1029/2009JC006075.

Pavelsky, T. M., M. T. Durand, K. M. Andreadis, R. E. Beighley, R. C. D. Paiva, G. H. Allen, and Z. F. Miller (2014), Assessing the potential global extent of SWOT river discharge observations, J. Hydrol., 519, 1516-1525, doi:10.1016/j.jhydrol.2014.08.044.

Pedinotti, V., A. Boone, S. Ricci, S. Biancamaria, and N. Mognard (2014), Assimilation of satellite data to optimize large-scale hydrological model parameters: a case study for the

SWOT mission, Hydrol. Earth Syst. Sci., 18, 4485-4507, doi:10.5194/hess-18-4485-2014.

Pitcher, L.H, Pavelsky, T.M., Smith, L.C., Moller, D.K., Altenau, E.H., Allen, G.H., Lion, C., Butman, D., Cooley, S.W., Fayne, J., and M. Bertram. (2019), AirSWOT InSAR mapping of surface water elevations and hydraulic gradients across the Yukon Flats Basin, Alaska. Water Resources Research, 55, doi:10.1029/2018WR023274.

QGIS Development Team (2020), QGIS Geographic Information System, Open Source Geospatial Foundation Project, http://qgis.osgeo.org.

Rodell, M., P. R. Houser, U. Jambor, J. Gottschalck, K. Mitchell, C.-J. Meng, K. Arsenault, B. Cosgrove, J. Radakovich, M. Bosilovich, J. K. Entin, J. P. Walker, D. Lohmann, and D. Toll (2004), The Global Land Data Assimilation System, Bull. Amer. Meteor. Soc., 85(3), 381-394.

Rodriguez, E. (2016), Surface Water and Ocean Topography Mission (SWOT) Project, Science Requirements Document, Rev A, 28 pp., https://swot.jpl.nasa.gov/files/swot/D-61923_SRD_Rev%20A_20160318%20with%20signatures1.pdf.

Sampson, K. and D. Gochis (2015), WRF-Hydro GIS pre-processing tools: Version 2.2 documentation, Tech. rep., Boulder, Colorado, 39 pages.

Senatore, A., G. Mendicino, D. J. Gochis, W. Yu, D. N. Yates, and H. Kunstmann (2015), Fully coupled atmosphere-hydrology simulations for the central Mediterranean: Impact of enhanced hydrological parameterization for short and long time scales, J. Adv. Model. Earth Syst., 7, 1693-1715, doi:10.1002/2015MS000510.

Skamarock, W. C., J. B. Klemp, J. Dudhia, D. O. Gill, D. M. Barker, M. G. Duda, X.-Y. Huang, W. Wang, and J. G. Powers (2008), A description of the Advanced Research WRF

513 version 3, NCAR Technical Note, 475, 113 pp.,
514 http://www2.mmm.ucar.edu/wrf/users/docs/arw_v3.pdf.
515 Strahler, A. N. (1957), Quantitative analysis of watershed geomorphology, Eos Trans. AGU, 38
516 (6), 913-920, doi:10.1029/TR038i006p00913.
517 U. S. Geological Survey (2017), National Elevation Dataset (NED),
518 https://nationalmap.gov/elevation.html.
519 Yoon, Y., M. Durand, C. J. Merry, E. A. Clark, K. M. Andreadis, and D. E. Alsdorf (2012),
520 Estimating river bathymetry from data assimilation of synthetic SWOT measurements, J.
521 Hydrol., 464-465, 363-375, doi:10.1016/j.jhydro.2012.07.028.
522 Yucel, I., A. Onen, K. K. Yilmaz, and D. J. Gochis (2015), Calibration and evaluation of a flood
523 forecasting system: Utility of numerical weather prediction model, data assimilation, and
524 satellite-based rainfall, J. Hydrol., 523, 49-66, doi:10.1016/j.jhydrol.2015.01.042.
525 Zhang, G., H. Xie, S. Kang, D. Yi, and S. F. Ackley (2011), Monitoring lake level changes on
526 the Tibetan Plateau using ICESat altimetry data (2003-2009), Remote Sensing of
527 Environment, 115 (7), 1733-1742, doi:10.1016/j.rse.2011.03.005.

List of Tables

List of Figures

548 **Tables**

549 Table 1. Noah-MP and WRF-Hydro parameterization options. More information about these
550 options are available in Niu et al. (2011) and Gochis et al. (2018).

Noah-MP Namelist Option	Namelist Value
Dynamic Vegetation Option	4
Canopy Stomatal Resistance Option	1
BTR Option	1
Runoff Option	3
Surface Drag Option	1
Frozen Soil Option	1
Supercooled Water Option	1
Radiative Transfer Option	3
Snow Albedo Option	2
PCP Partition Option	1
TBOT Option	2
Temp Time Scheme Option	3
Glacier Option	2
Surface Resistance Option	4
WRF-Hydro Namelist Option	
Channel Routing Option	3 (Diffusive wave gridded)
Groundwater/Baseflow Routing Option	1

551

552 **Figures**

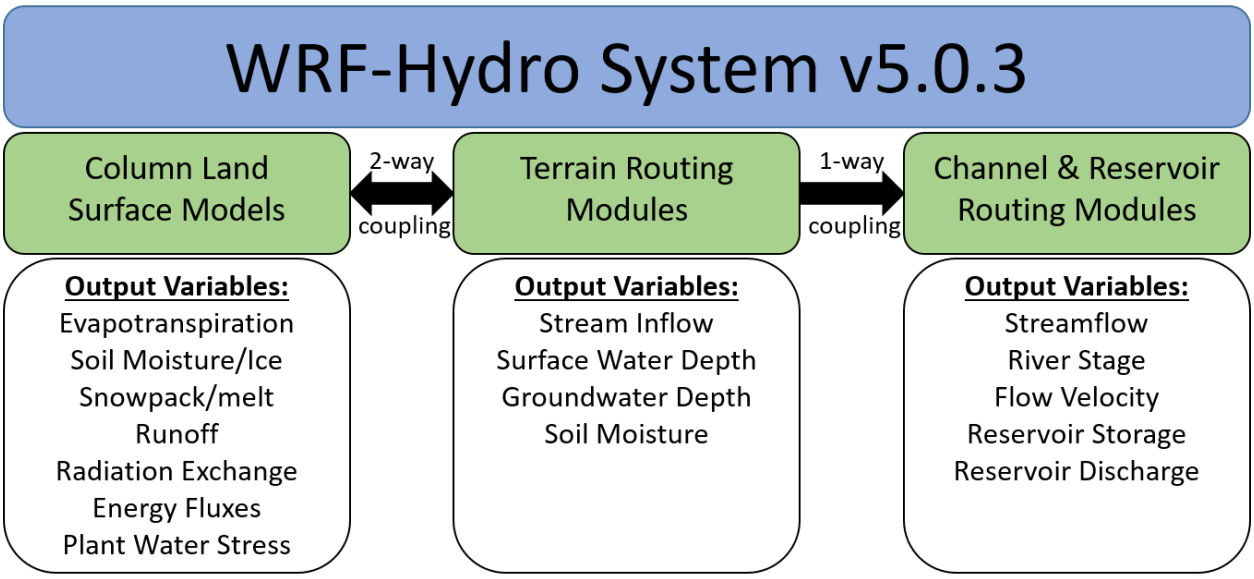

553
554 Figure 1. WRF-Hydro version 5.0.3 modules and output variables when coupling with an

555 atmospheric model is disabled.

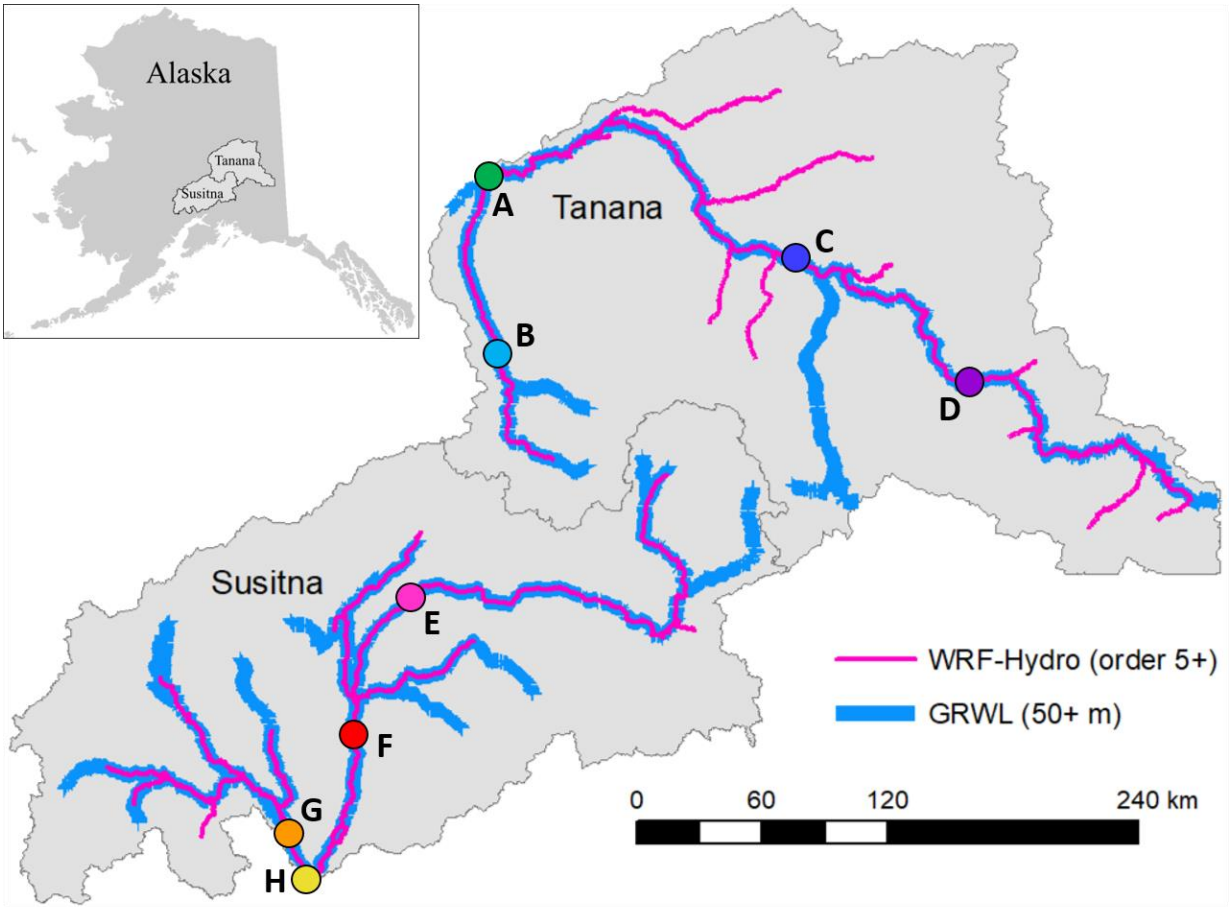

556

557 Figure 2. Comparison of WRF-Hydro streamorder estimate of river width (magenta lines) to
558 GRWL rivers widths greater than 50 m (blue lines) which will observable by SWOT. Basin
559 extents are indicated in gray. Letters and colored dots refer to hydrographs in Figure 5.
560

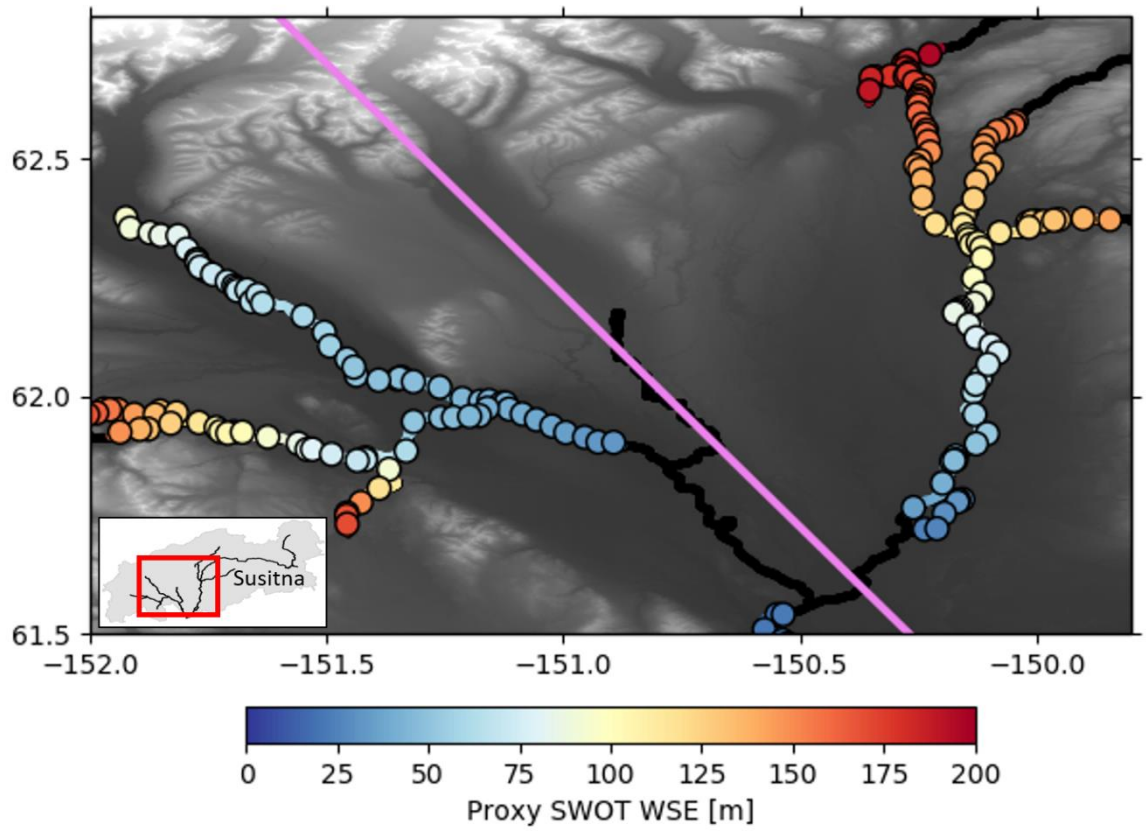

Figure 3. 1100 UTC 22 September 2012 reach-level $WSE'_{WRFHydro}$ (colorbar) for the Susitna River basin along with the proxy SWOT ground track (violet), the unobserved channel network (black), and topography (background, grayscale).

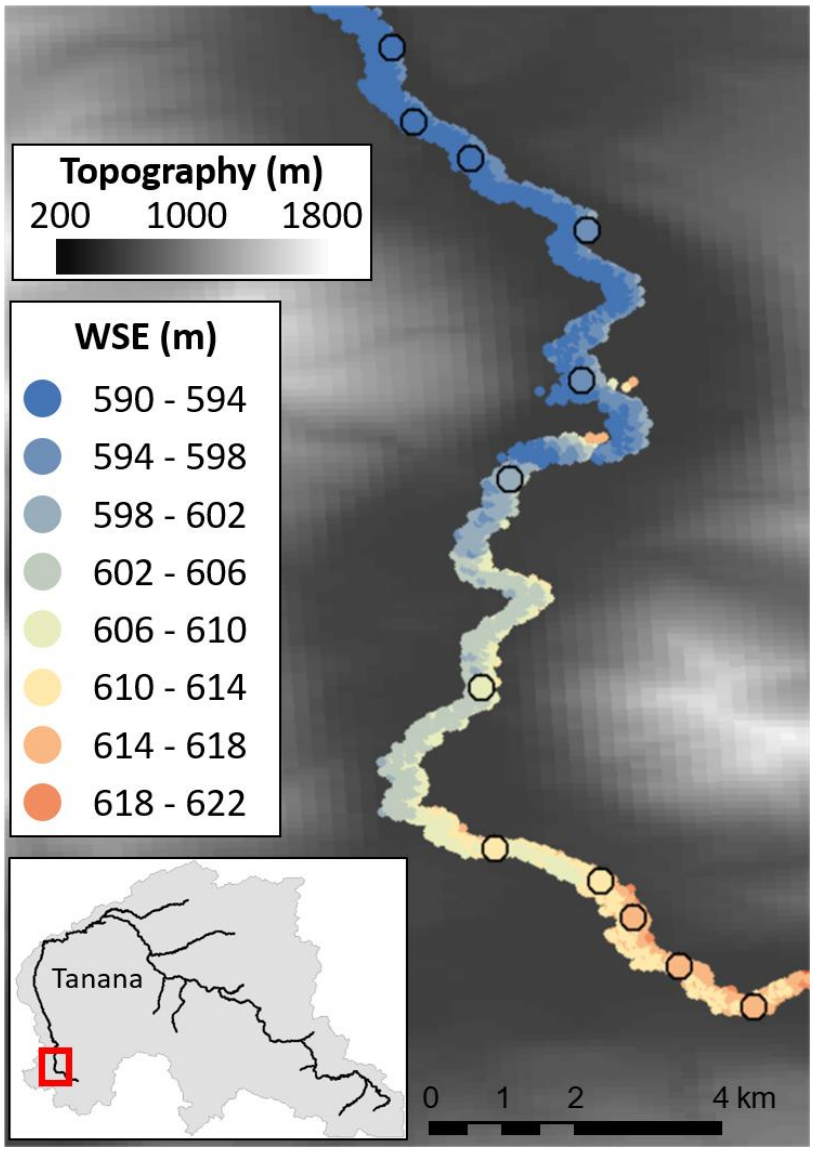

565

566 Figure 4. Example of CNES simulator output comparing WSE'_{PixC} (small circles, no outline),

567 and $WSE'_{ReachAvg}$ (large circles with black outline). WRF-Hydro output from 1 June 2015 is

568 used as input to the CNES simulator. Grayscale background depicts the WRF-Hydro topography.

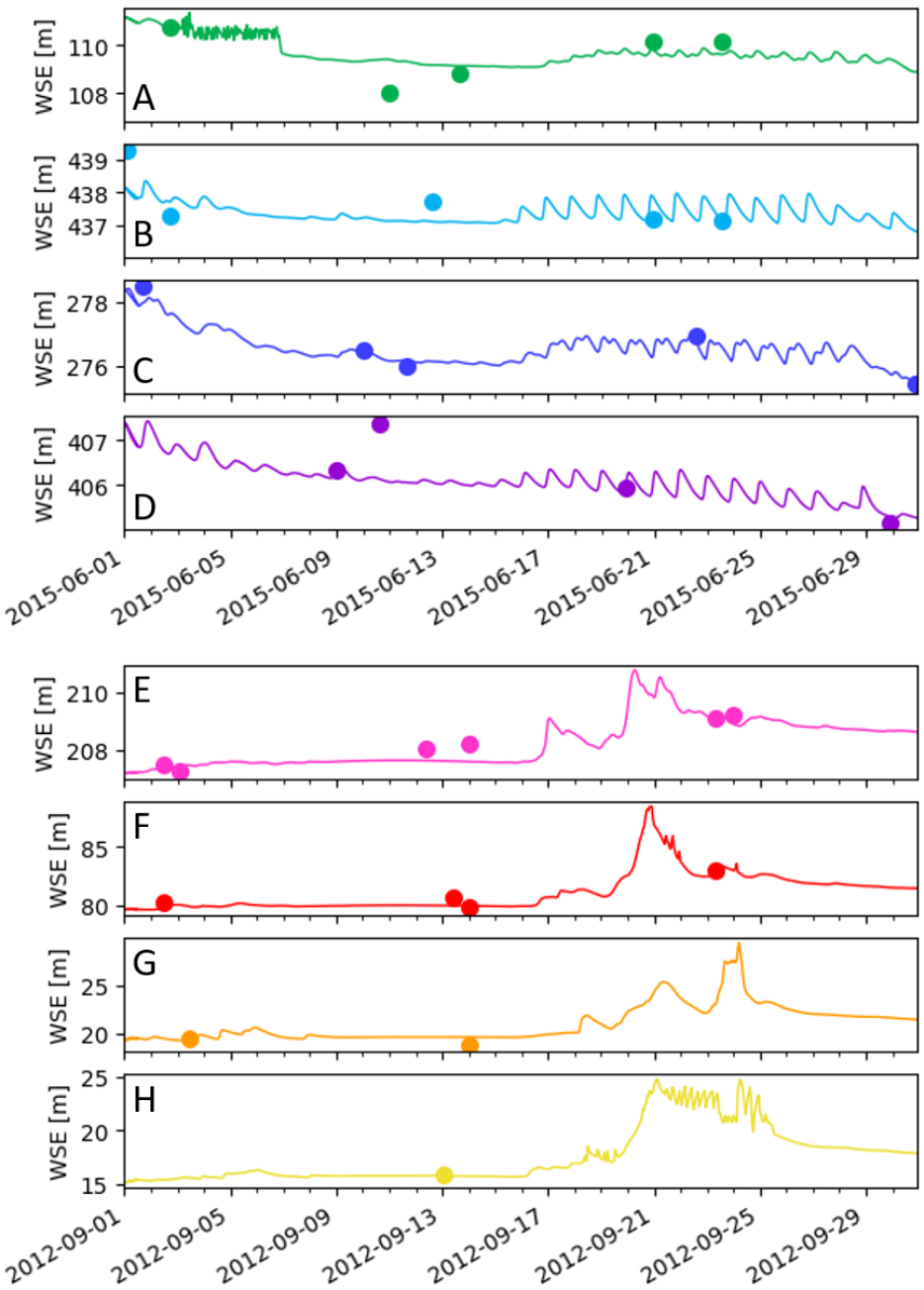

569

570 Figure 5. Hydrographs comparing WSE_{True} (lines) and $WSE'_{ReachAvg}$ (points). Letters and

571 colors correspond to points shown in Figure 2.